Research Article

SOHAG JOURNAL OF SCIENCES

https://doi.org/10.21608/sjsci.2023.187375.1056

Intrusion-related Low Sulphidation Gold Mineralization, Wadi Hammad Area, North Eastern Desert, Egypt

Ahmed El-Sheikh*, Mohamed Ali, ElSayed A. Saber

Geology Department, Faculty of Science, Sohag University, Sohag 82524, Egypt.
**E-mail:ahmed_abdelrashid@science.sohag.edu.eg; alschaikh@yahoo.com*

Received: 1st January 2023, **Revised:** 20th January 2023, **Accepted:** 21st January 2023.
Published online:1st May 2023

Abstract: Gold mineralization in Wadi Hammad is one of few gold occurrences located in the North Eastern Desert of Egypt, occurring at the boundary between the post-tectonic Younger granite and Dokhan volcanics along a north-south (N-S) trending shear zone between them. The main mineral assemblages include arsenopyrite-pyrite-chalcopyrite-galena-sphalerite and sphalerite-gold-covellite-cerussite-pseudomorphic iron oxides. Mineralogical and geochemical studies indicate that the mineralization is of the low sulphidation epithermal gold type, with Pb-Cu type base-metal sulfides. The hydrothermal solutions forming the mineralization have temperatures between 200 and 300 °C. The mineralization formed in three main stages; the first one includes the intrusion of younger granite into the Dokhan volcanics coeval with the initial shearing along the contact between them and responsible for the formation of the main milky white quartz–polymetallic sulfide vein. The second stage is related to later (third and fourth) deformational events responsible for the formation of the grey-colored quartz hosting sphaleriteII-gold-covellite-cerussite-pseudomorphic iron oxides and connected with the basic dolerite dykes and related hydrothermal solutions. This stage includes the release of gold from their main sulfide hosts and re-precipitation in the fractures in quartz vein and alteration zones. The results of this study reveal the existence of promising gold deposits in the North Eastern Desert (NED) of Egypt, which changes the stereotype and may set the stage for future exploration of gold in the NED. Moreover, this study unveiled the nature of the intrusion-related type of mineralization and their characteristic features which can be used in the exploration of similar types in the surrounding areas.
Keywords: Hammad deposit, shear zone, hydrothermal mineralization, epithermal, and gold-base-metal.

1. Introduction

Gold deposits that show close association in time and space with I-type calc-alkaline to alkaline granitic magmatism, commonly in the post-collision environment within the continental margin or during the extensional period in convergent regimes are categorized as intrusion-related gold deposits [1]. In Egypt, intrusion-related gold deposits with other metal mineralization are related to the emplacement of the calc-alkaline and alkaline granites at (610–590 Ma), and contemporaneous eruption of the late-orogenic Dokhan volcanic and deposition of Hammamat sediments, coeval with the activity of the Najd fault system [2, 3]. Intrusion-related gold deposits in the Eastern Desert of Egypt are represented by Au-bearing quartz veins and/or hydrothermally altered zones hosted within (1) post-collisional granites or in the contact with (2) younger gabbros, (3) Dokhan volcanic, (4) Hammamat sediments, (5) ophiolitic serpentinites, and (6) island arc assemblages and ophiolitic mélange. The majority of these mineralizations are widely distributed in the Central and Southern Eastern Desert of Egypt, whereas their occurrences in the Northern Eastern Desert are very limited and poorly studied[4].

In the Hammad gold deposit which is located in the North Eastern Desert, the gold-bearing quartz vein occurs in the contact between the post-collisional granites and the Dokhan volcanic. The deposit was poorly studied and has limited research attention e.g., [5-7]. According to these studies, fracturing and shearing of the wall rocks are the main factors controlling the alteration and mineralization where galena and pyrite are the main primary sulfides while sphalerite and chalcopyrite are subordinate [5]. Galena (the main primary host of electrum) has been altered with other sulfides into carbonates and oxides while Ag and Au were leached out and precipitated in the form of low-Ag gold[8]. Gold was formed in two stages: primary hydrothermal gold, and secondary gold related to the oxidation of preexisting Au-bearing minerals [6]. Fire Assay analyses of gold up to 50 g/t (average 6.7 g/t) in quartz veins and up to 199 g/t (average 23.3 g/t) in the alteration zone were recorded [7]. As mentioned before, the present Hammad deposit is poorly studied and needs more detailed work and investigation to determine the mineralization style, mineralogy, and geochemistry of the host rocks and the ore deposit, to decipher the type of mineralization and mode of formation.

2. Geological and Structural Settings of Hammad area

The Hammad area is located at the western boundary of the Arabian-Nubian Shield and lies between latitudes26°58′ and 27°10′ N and the longitudes 32°50′ and 33°02′ E (Fig. 1A). The WadiHammadexists to the west of GabalDokhan and to

the southeast of Gulf granitic mass. Various volcanic and plutonic rocks of Neoproterozoic age are exposed in the area; they are arranged from older to younger as follows:

(Younger)	Post granitic dykes
	Younger Granites (G2)
	Hammamat sediments
	DokhanVolcanics
(Older)	Metagabbro- diorite complex

2.1. Dokhan Volcanics and Hammat sediments:

The Dokhan Volcanics and Hammamat sediments are represented by a NW–SE-trending belt preserved overlying the older granites and low-grade metasediments and metavolcanics [**9, 10**]. The belt is intruded by younger granites and sub volcanic intrusions of sill- and dyke-type (Fig. **2A**)

2.1.1. Dokhan Volcanics

The Dokhan Volcanics constitute a thick sequence of moderately high mountainous ridges. The investigated volcanic rocks are represented by two units:

(a) Lower Dokhan Volcanic suite, represent by intermediate lava flow and their pyroclastic intercalations, this type of volcanic rocks croup out mostly along the northeastern and southwestern parts of the area; the intermediate Dokhan volcanic suite represented by porphyritic andesite and their pyroclastics (Fig. **2B**).

(b) Upper Dokhan Volcanic suite, represented by felsic lava flow and inter-bedded felsic pyroclastics. The felsic rocks crop out at the northwestern part of the area and the Wadi Hammad mine locality. The rocks of this suite are mainly porphyritic rhyolite, dacite, and rhyodacite, in addition to felsic tuffs and ignimbrite (Fig. **2C**).

2.1.2. Hammamat Group

The Hammamat sediments bound the Dokhan volcanic from the south. The contact is intercalations of the two units where the upper part of the older Dokhan Volcanics is intercalated with greywacke and conglomerate of the overlying Hammamat sediments. The Hammamat sediments are represented by thickly bedded succession, about 8 m thick of siltstones, greywacke, and conglomerate.

2.2. Intrusive rocks

The intrusive rocks in the Hammad area are represented by granitic rocks. These granite rocks are well exposed along the western bank of Wadi Hammad and at Gabal El-Guluf. Published report [**11**] mentioned that these granites form high rough mountains with sharp, rugged peaks and are dissected by elongated gullies with steep walls. From the eastern margin granite mass intrudes the Dokhan Volcanics and the contact is steeply inclined toward the east, the granitic rocks along the contact takes enclaves from the Dokhan Volcanics. The granitic rocks are younger than the volcanic rocks [**12**]. This is indicated by the contact relationship, xenoliths and enclaves of

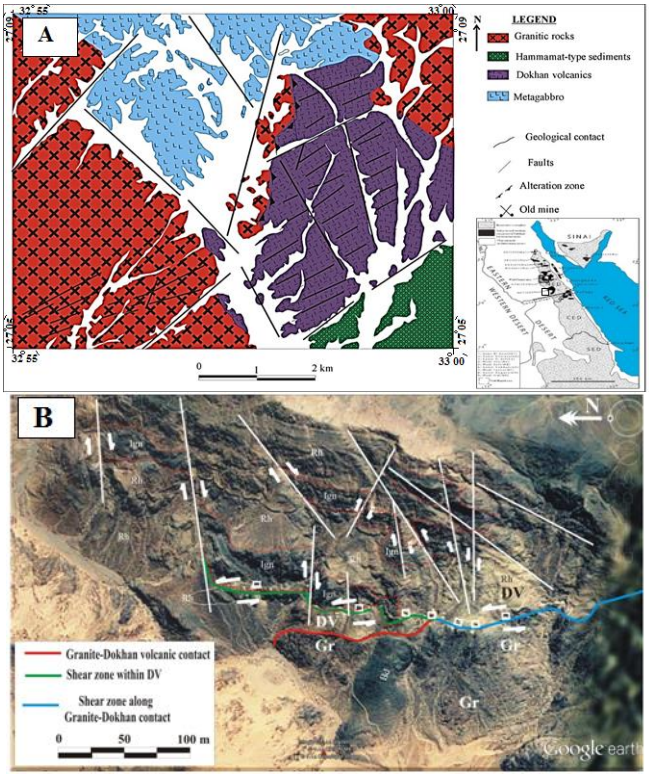

Figure 1. A) Geological map of Wadi Hammad area; B) Google Earth image showing the main rock units, structures, and site of mineralization. Rock units at the outcrop comprise Dokhan Volcanics (DV) of ignimbrite (Ign), and rhyolite (Rh); Gr=post tectonic granite and basic dyke(Bd).

volcanic rocks within the plutonic rock (Fig. **2D**). To the western side of Wadi Hammad and in the southern part of the granitic mass, the granite rocks intruded Hammamat sediments (conglomerates, Fig. **2E**). The granitic rocks are well-jointed and dissected by numerous faults and shear zones.

2.3. Structure controls

Wadi Hammad area represents a pull-apart basin, it is 15 km in length and 9 km in maximum width[**13**]. This basin was formed due to regional extensional and strike-slip tectonics after the orogenic events that formed the Pan-African Belts [**14**]. Wadi Hammad area seems to have been subjected to many superimposed deformational tectonic events [**15**]: The first is a compression force, in the N65ºE direction, causing two sets of conjugate faults: one set of E-W sinistral faults and another set of NE-SW trending normal faults dextral faults (Fig. **1B**). The second event was also compressional, whose axis of maximum compression σ2 trends in the N25ºE direction, causing two sets of conjugate shear zones; one set of N-S sinistral shear zones and another of NW-SE dextral shear zones. The N-S sinistral shear zones trending shear zone hosts the main Pb-bearing auriferous quartz vein along or close to the contact between younger granites and Dokhan Volcanics; more inside the latter (Fig. **2F**). This is the most important structural feature in Wadi Hammad area representing a ductile shear zone, of about 1 km long and consists of highly sheared rocks mainly of mylonites (Fig. **2G**). The most common shearing fabrics observed in the host and wall rocks include S-

C structures (see Fig 2H). The third event is extensional dextral faulting and shearing in the ENE-WSW direction, causing displacement of the mineralized zone and the contact and between the younger granites and Dokhan Volcanics. This extension is represented in the mine area by basic dolerite dykes that crosscut the mineralized quartz vein in the central and southern parts of the mineralization area (see Fig. 1B). The fourth event was also compressional, in the N40ºW direction causing the formation of two conjugate sets of shear fractures sets trending WNW-ESE dextral faults and shearing and NNW-SSE sinistral faults and shearing. This has led to dextral shearing inside the quartz veins in the WNW-ESE direction (Fig. 2H). Effects of these superimposed shearing on the milky white quartz vein lead to development of laminated grey colored Au-rich quartz veins (Fig. 2I).

The study area is thus cut by NE and ENE trending dextral strike slip faults along the northeastern and southwestern margins. It is cut by NW-trending normal faults along the northwestern and southeastern part of the mapped area (Fig.1). The area dissected by a number of interbasinal NE-trending strike-slip faults and E-W-trending faults. These faults are responsible for intense deformation, marked by the steepening to nearly 90°and a high density of minor faults in broad fault zones. The ENE, NW, N-S and E-W are the dominant trends of faults recorded in the study area.

4. Material and methods

Field work includes description and measuring of the main mineralization and collecting representative samples of the country rocks and associated ore deposits in the studied. For petrographic investigation, more than 30 thin polished sections were prepared in the laboratory of rocks and minerals in Assuit University. The petrographic study was achieved using a transmitted and reflected light Polarizing Microscope. Semi-quantitative analyses for selected minerals were analyzed with the scanning electron microscope (SEM) and energy dispersive spectrometer unit (EDS) of some polished surfaces of the selected ore samples; SEM and EDS analyses were carried out by using SEM model Philips XL30. The analytical conditions were 30 kV accelerating voltages, 1–2-µm beam diameter, and 60–120 s counting times. Minimum detectable weight concentration from 0.1 wt% to 1 wt%, precision well below 1%, the relative accuracy of quantitative result 2%–10% for elements Z>9 (F), and 10%– 20% for the light elements B, C, N, O and F. The analyses were carried out at laboratories of the Egyptian Nuclear Materials Authority (NMA).

Chemical analyses of 12 samples of granitic rocks and 23 samples of Dokhan volcanics were carried out at the Central Laboratories of the Geological Survey of Egypt. The chemical composition of both major (in wt %) and trace elements (in ppm) was performed by using a Philips x-ray fluorescence technique model PW/2404, with Rh radiation tube. Detection limits for major oxides are between 0.001 and 0.03%, and detection limits for trace elements are between 0.01 and 0.5 ppm. Loss on ignition (L.O.I) of samples was obtained by heating 0.5 g of powdered sample at 1000 °C overnight. 18 samples of the ore deposits were analyzed to determine main contents using the inductively coupled plasma-mass spectrophotometry technique (ICP-MS)

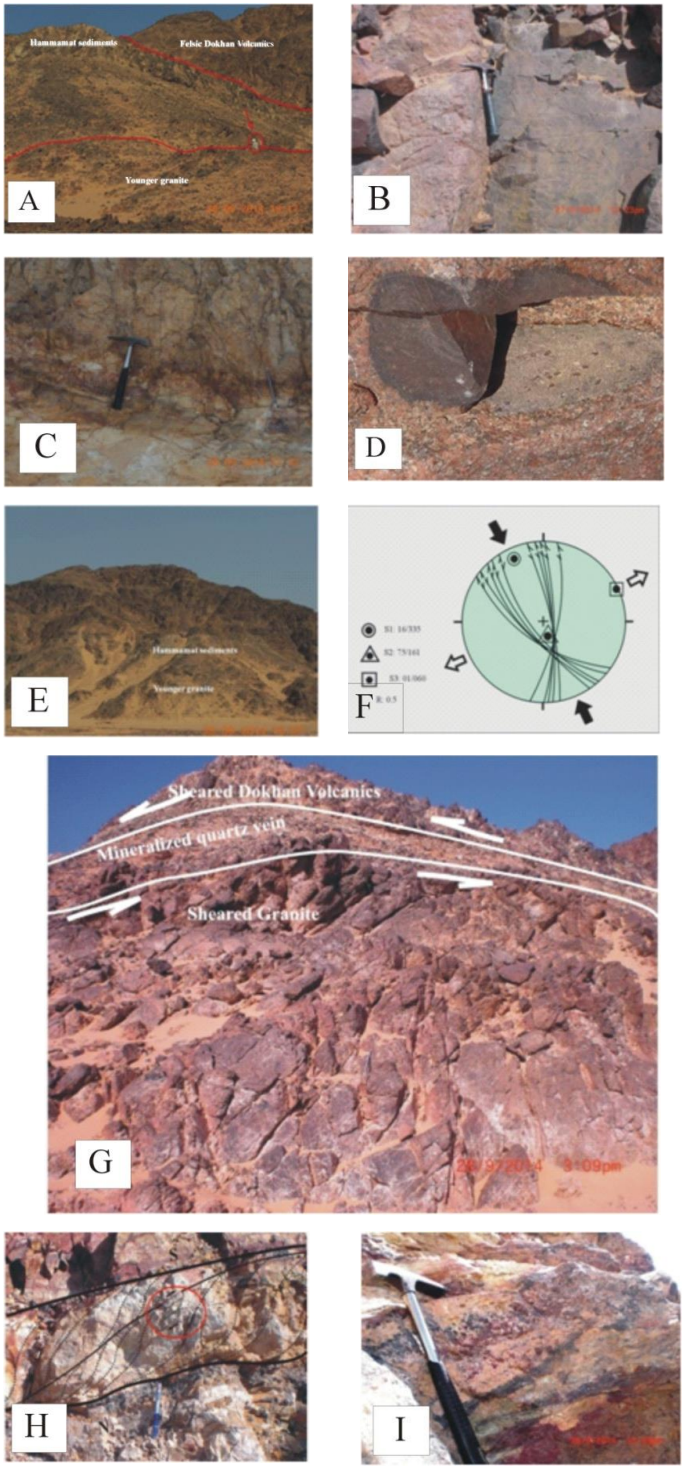

Figure 2. A) Dokhan Volcanics and Hammamat sedimentsintruded by younger granites, Wadi Hammad area; B) Sharb contact between the intermidiateDokhan Volcanic and Younger granite, Wadi Hammad area; C) ignimbrite, Upper Dokhan volcanic suite, Wadi Hammad area; D) Younger granite contains enclaves of volcanic rocks, Wadi Hammad area; E) Younger granite rocks intruded Hammamat sediments (conglomerates), western side of Wadi Hammad area; F) Sinestral N-S trending main shear zone hosting the mineralized quartz vein; G) Sinestral N-S trending main shear zone hosting the mineralized quartz vein; H) S-C surfaces dextral sense of shear in the sheared mineralized quartz vein.; I) Banded grey colored mineralized quartz developed inside the main quartz vein.

(720 ICP-OES, Agilent Technologies), with Detection limits 0.1 ppm, carried out at the Central Laboratories of the Geological Survey of Egypt.

5. Results

5.1. Lode geometry and mineralization styles

Three modes of occurrence of the polymetallic mineralization in Wadi Hammad area; they are 1- mineralized quartz vein, 2- hydrothermal wall rock alteration and 3- breccia. The mineralized quartz vein, silicified shear zone and the associated hydrothermal alterations are mainly confined to and controlled by Wadi Hammad shear zone. Quartz vein occurs in the center of the shear zone and ranges in width from 80 centimeters in the southern part, decreases in thickness towards the north to about 10 centimeters until disappear completely in the most northern part, it extends for about 500 meters along the strike of the shear zone (Fig. **3A**). In the southern part, the quartz vein is thick and generally is composed of white to smoky quartz. This part shows vuggy, colloform and comb structures (Fig. **3B**). The mineralization is represented by massive, disseminated, vuggy filling and fracture filling sulfides in the quartz vein. In the northern part the thickness of quartz vein is about 5-10 cm, it is massive and not mineralized. The hydrothermal processes resulted in the formation of alteration zones around the mineralized quartz vein (Fig. **3C**). Five-meter width zone of hydrothermal alteration surrounding the mineralized quartz vein has been affected by the structural features in the host rocks. Two distinct alteration zones are recognized according to proportions of the developed hydrothermal/secondary minerals. The alterations around the quartz vein in the studied area have unique mineral assemblages, but in many cases they show an overlapping. The presence of alteration minerals such as, sericite, secondary muscovite, kaolinite, pyrite, and secondary quartz indicates simultaneous sericitic, quartz– chlorite–epidote–pyrite alterations and silicification. Most of the alteration minerals are replaced by sulfide minerals (e.g. pyrite, sphalerite, chalcopyrite ...ect).

The shear zone around the quartz vein is reddish in color due to highly oxidized base metal sulfides and formation of ferruginous materials (hematite overprint, Fig. **3D**). Beside the main quartz vein, silicification in the shear zone is represented by small quartz veinlets/selvages (Fig. **3E**)**.** Breccia type; based on clast lithology, size, shape and cement composition, three types of breccia are recognized: Breccia I, II and III. Breccia I composed of angular to subangular clasts of host rocks, their size ranges from 1 to tens of cm. The clasts are embedded in fine- to coarse-grained quartz, this type of breccias occurs mainly close to the contact between the Dokhan Volcanics and the intruded younger granite. The rock clasts derived mainly from Dokhan Volcanic (Fig. **3F**). Breccia II consists of subrounded to subangular very coarse-grained clasts of altered country rocks. Components set in siliceous and iron oxide and hydroxide rich cement, breccia II is located adjacent to the quartz vein and mainly cut by numerous quartz and sulfide veinlets (Fig **4A**). Breccia III, two subtypes of breccia III can be distinguished based on the cement composition. The first type is Breccia IIIa, composed of fine to medium-grained

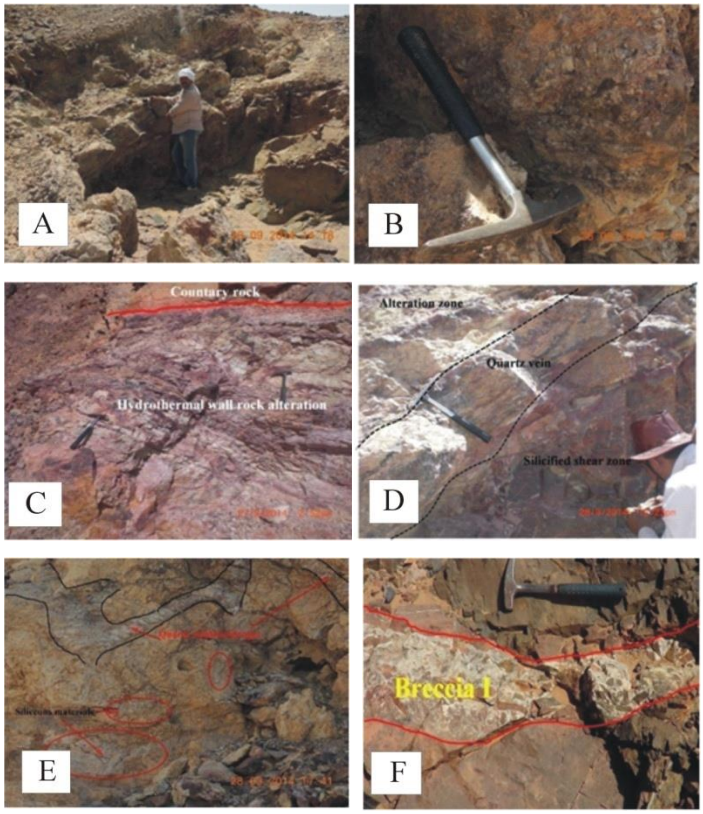

Figure 3. A) Quartz vein runs in the center of the shear zone; B) Vuggy, colloform, and comb structures of quartz vein, C) Alteration zone around quartz vein, Wadi Hammad area; D) red color Silicified shear zone; E) shear zone is cut by quartz veinlets/selvages; F) Breccia I composed of angular to subangular clasts derived from Dokhan Volcanic sit in fine- to coarse-grained quartz cement.

quartz clasts and fragments of about 0.5 to 3 cm in length. The quartz fragments suffered from shearing and deformation. The clasts components cemented by ferruginous material of iron oxide; this type of breccia occupies the marginal part of the main quartz vein (Fig. **4B**). Breccia IIIb is composed of quartz fragments of angular to subangular shape ranging from 2mm to 5mm. The clast components are cemented by sulfide minerals mainly sphalerite and galena (Fig. **4C-F**). This type of breccia occupies the central part of the main quartz vein.

5.2. Mineralogy and Micro-chemical analysis

Arsenopyrite occurs mainly in the milky quartz vein where it is not detected in the wall rock alteration, it forms euhedral to subhedral prismatic crystals of about 3 to 5 mm in length and about 2 to 3 mm in width (Fig. **5A**). Arsenopyrite oxidizes to iron oxides along their grain boundaries and fractures. Selective oxidation of particular zones in arsenopyrite indicates zoning in the original grains (Fig. **5B**). Locally arsenopyrite consists of two zones; the inner zone contains a large number of galena or intergrowth of galena, sphalerite, and chalcopyrite (Fig. **5C**). It is frequently associated with coarse grained pyrite and disseminated chalcopyrite, galena and fine-grained sphalerite. Arsenopyrite composition according to EDS analysis is: As (39.08 wt%), Fe (36.31 wt %), S (23.36 wt %), and O (2.82 wt%), (Fig. **6A**).

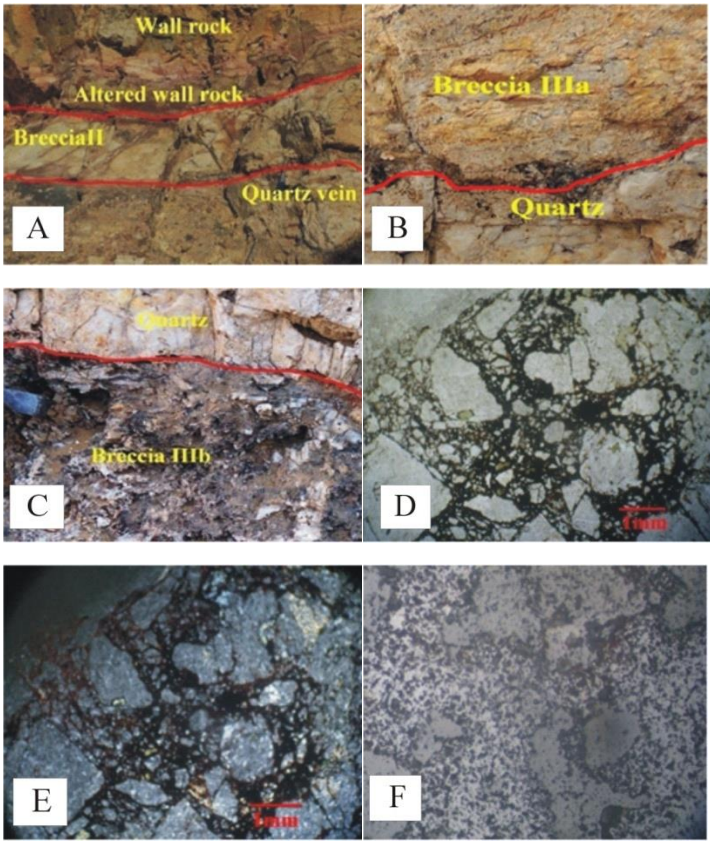

Figure 4. A) Breccia II consists of very coarse-grained clasts of altered country rocks sit in siliceous cement; B) Breccia IIIa, composed of fine to medium-grained sheared quartz clasts cemented by ferruginous material of iron oxide; C,) Breccia IIIb composed of angular to subangular quartz fragments cemented by sulfide minerals mainly of sphalerite and galena; D, E, and F) Photomicrograph showing breccia III under transmitted, CN polarized light PPL,cross nikols CN and reflected light respectively.

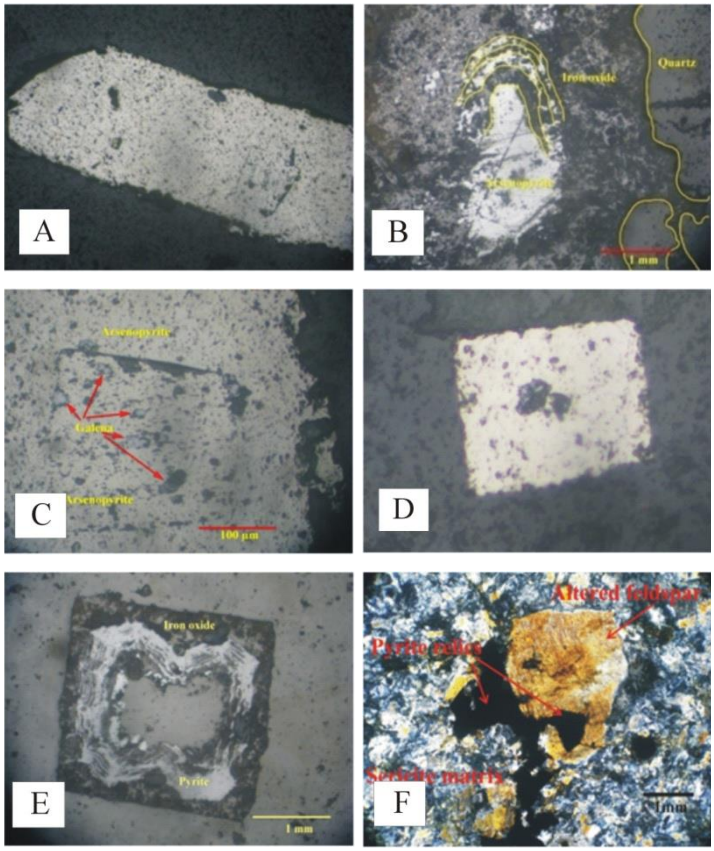

Figure 5. A) Euhedral to subhedral prismatic aresnopyrite; B) Selective oxidation of particular zones in arsenopyrite; C) Arsenopyrite consists of two zones; the inner zone contains a large number of galena; D) Pyrite-I disseminated in quartz vein; E) Zoning and variable oxidation of pyrite-I to pseudomorphic iron oxide; F) Pyrite-II is formed along the cleavage planes of plagioclase.

Pyrite is found in two main types, namely Pyrite-I and pyrite-II. Pyrite-I occurs mainly in the quartz vein and pyrite-II occurs mainly in the altered wall rocks. Pyrite-I forms coarse-grained disseminated cubes of about 4 mm in diameter (Fig. **5D**), the individual cube shows zoning indicated by variable oxidation to pseudomorphic iron oxide (Fig. **5E**), sometimes the pyrite cubes are partly to completely altered to iron oxide and only relics of pyrite can be observed, the oxidized part in zoned pyrite contains fine-grained gold. Pyrite-II is formed along with alteration minerals; epidote, muscovite, chlorite, and along the cleavage planes of plagioclase (Figs. **5F**, **7A**, **7B**, **7C**). Pyritization of these minerals is one of the most widespread phenomena in altered wall rock, in which pyrite-II formation starts as very fine-grained and then grows to form very coarse-grained cubes which can be observed by the naked eye (Fig. **7D**). This pyrite-II and its oxidation products are characterized by their presence as skeletal crystals (Fig. **7B**) and presence of relics of the original silicate minerals which distinguish it from the Pyrite-I type (Figs. **8E** and **8F**). The composition of pyrite as indicated by EDS analyses is Fe (39.01 wt %), S (45.84 wt %), Si (6.88 wt%), and O (8.27 wt %) (Fig. **6B**).

Chalcopyrite is one of the most abundant sulfide minerals in the Hammad ore deposit, it forms subhedral and anhedral fine- to medium-grained crystals of about 30 to 40 µm across, disseminated in quartz vein (Fig. **8A**). It also occurs as inclusions within arsenopyrite and pyrite-I associated to and/or intergrown with fine grained galena and sphalerite. In both cases, chalcopyrite is altered along its grain boundaries to covellite and bornite (Fig. **8B**).

Chalcopyrite, covellite, and bornite are all later oxidized into malachite which stained the mineralized quartz vein with green color (Fig. **8C**). EDS analysis show a composition of chalcopyrite (Fig. **6C**) as Cu (48.76 wt %), Fe (29.75 wt %), S (10.48 wt %), O (8.18 wt%) and Ni (2.82 wt %).

Galena occurs as a medium- to coarse-grained cubes ranging in size from 1mm to 0.5 cm), disseminated in the quartz vein and can be observed by the naked eye (Fig. **8D**). Galena cubes are partly to completely altered to cerussite, along its boundaries and cleavages with relict islands of galena (Fig. **8E**). Galena is commonly associated with the fine grained sphalerite and chalcopyrite in quartz vein and as inclusions inside the arsenopyrite (Fig. **8F**).

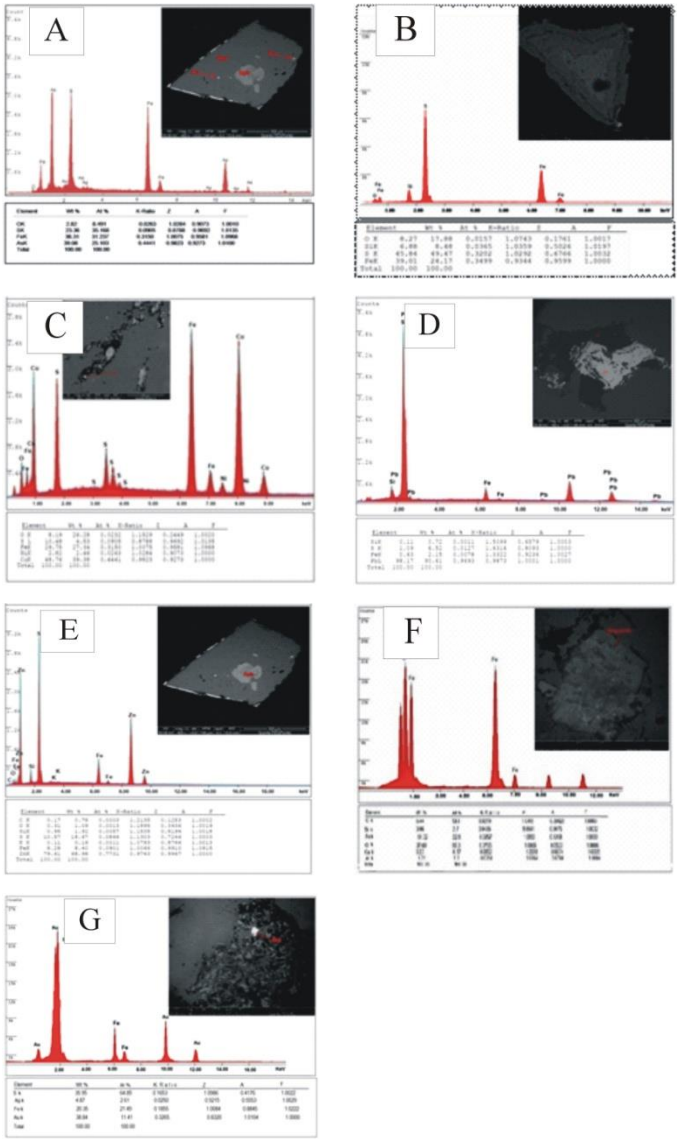

Figure 6. EDS spectra and back-scattered images of; A) Arsenopyrite; B) Pyrite; C) Chalcopyrite; D) Galena; E) Sphalerite; F) Magnetite; and G) Gold, from mineralization in Wadi Hammad area.

Galena is rarely observed in the altered wall rocks, it occurs as euhedral cubes disseminated in silicate groundmass. EDS analyses of galena (Fig. **6D**) indicates that it is made up of Pb (98.17 wt %), S (1.09 wt %), Fe (0.63 wt %), and S (0.11 wt %).

Sphalerite is the most common sulfide ore mineral in the Hammad area, it was recognized in both quartz vein and wall rock alteration. It occurs in two distinct types, namely sphalerite-I, and sphalerite-II. Sphalerite-I occurs in quartz vein as euhedral to subhedral, dark grey, fine-grained crystals, their size ranges from 20 to 30 µm. It is found as disseminated crystals in the massive milky quartz (Fig. **9A**) and as inclusions within the coarse-grained pyrite and arsenopyrite(Fig. **9B**). Sphalerite-I occasionally makes intergrowths with galena and chalcopyrite in quartz or within the coarse-grained arsenopyrite.

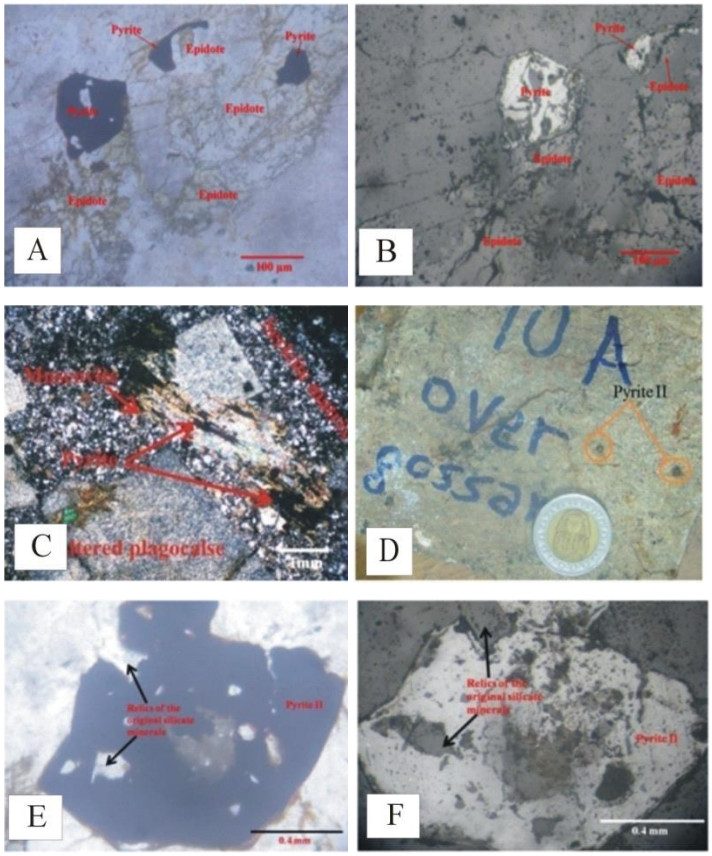

Figure 7. A) Photomicrograph showing pyrite-II is formed on the expense of epidote, under transmitted light; B) Photomicrograph showing pyrite-II formed on the expense of epidote and characterized by their presence as skeletal crystals, under reflected light; C) Pyrite-II is formed on the expense of muscovite; D) Very coarse-grained cubes pyrite-II which can be observed by the naked eye; E) Pyrite-II contains relics of the original silicate minerals, under transmitted light; F) Pyrite-II contains relics of the original silicate minerals, under reflected light.

Sphalerite-II is generally lighter in color than sphalerite-I and occurs in both the quartz vein and the alteration zone. In the quartz vein, sphalerite-II occurs in the form of coarse-to medium-grained crystals, fissure- and/or cavity-filling in the sheared quartz. This type is common in the central part of the main quartz vein where large cavity-fillings of sphalerite-II up to 50 cm wide were observed (Fig. **9C** and **9D**).In these situations, sphalerite-II cements the quartz clasts and fragments, which appear to float in a matrix of the former, and their grain boundaries are corroded by sphalerite (Fig. **9E**).

In altered wall rocks, sphalerite-II shows various textures, it occurs in the form of pseudomorphic euhedra, coarse-grained, 2 to 3 mm across, in silicate groundmass (Fig. 9F). Fracture-filling sphalerite-II forms vein- and veinlet-like textures; it ranges from few mm to more than 3 cm in width. Sphalerite-II contains rock fragments of variable sizes and shapes of the country rocks (Fig. **10A**). However, sphalerite minerals also selectively replace the wall-rock clasts and along fractures and zones of weakness (Fig. **10A**). In places, the wall-rock clasts seem to be cemented together by the sphalerite-II. Sphalerite-II

occasionally shows different shades of brown to reddish coloration particularly when passes through or close to pyrite and/or magnetite crystals (Figs. **10B**, **10C**, and **10D**). EDS analyses of sphalerite (Fig. **6E**) indicates that the main composition is represented by Zn (79.61wt%) S (10.57wt%) and Fe (8.28 wt%).

Magnetite is observed in the altered wall rock in both the plagioclase phenocrysts and in the groundmass (Figs. **10E** and 10F). It is found as individual cubes or aggregates of euhedral equant cubes, and its grain size is variable from fine to coarse-grained. The coarse-grained type is altered to hematite (i.e., martite) along grain boundaries and crystallographic planes; the hematite in turn was replaced by pyrite during the hydrothermal stage (reducing), particularly in the alteration zone where plagioclase is severely sericitized (Fig. **10E**).EDS analysis of magnetite indicate a composition of Fe (51.32 wt %) O (37.60 wt%), C (6.44 wt%), Si (3.06 wt%), Al (1.31 wt%) and Ca (0.27 wt%) (Fig. **6F**)

Gold occurs in both quartz vein and altered wall rocks in variable textures and sizes. Gold occurs in three distinct situations; (1) Disseminated in the quartz vein gold occurs in the form of fine grained nuggets 5-20 µm across (Figs. **11A** and **11B**), and is associated with quartz clasts in the breccia zone (Figs.**11C** and **11D**), (2) In the oxidation zones of the

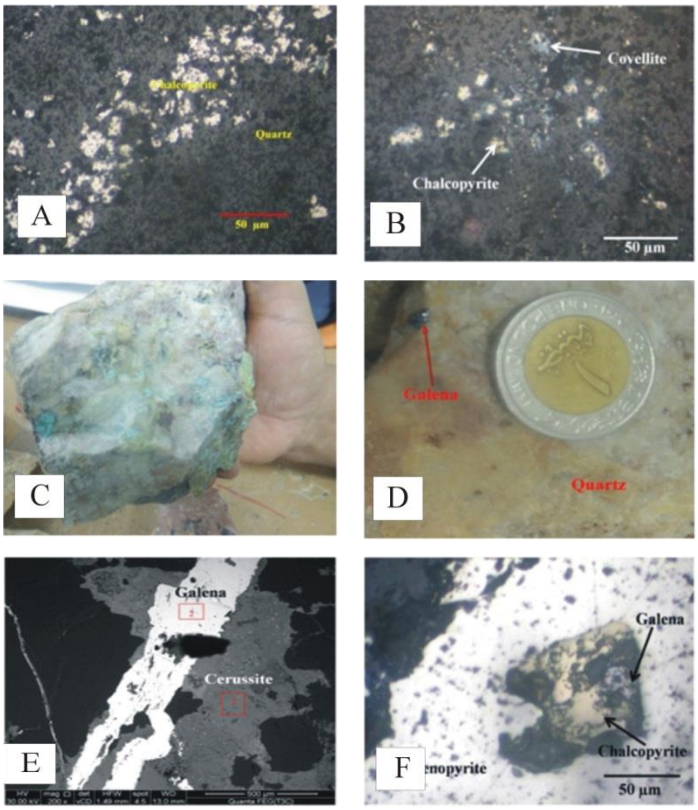

Figure 8. A) Subhedral and anhedral fine- to medium-grained chalcopyrite crystals, disseminated in quartz vein; B) Chalcopyrite is altered along its grain boundaries to covellite;C) malachite stained the mineralized quartz hand specimen with green color; D) Galena occurs as a medium- to coarse-grained cubes, disseminated in the quartz vein and can be observed by the naked eye; E) back-scattered image showing alteration of galena to cerussite; F) Galena is associated by chalcopyrite as inclusions inside the arsenopyrite.

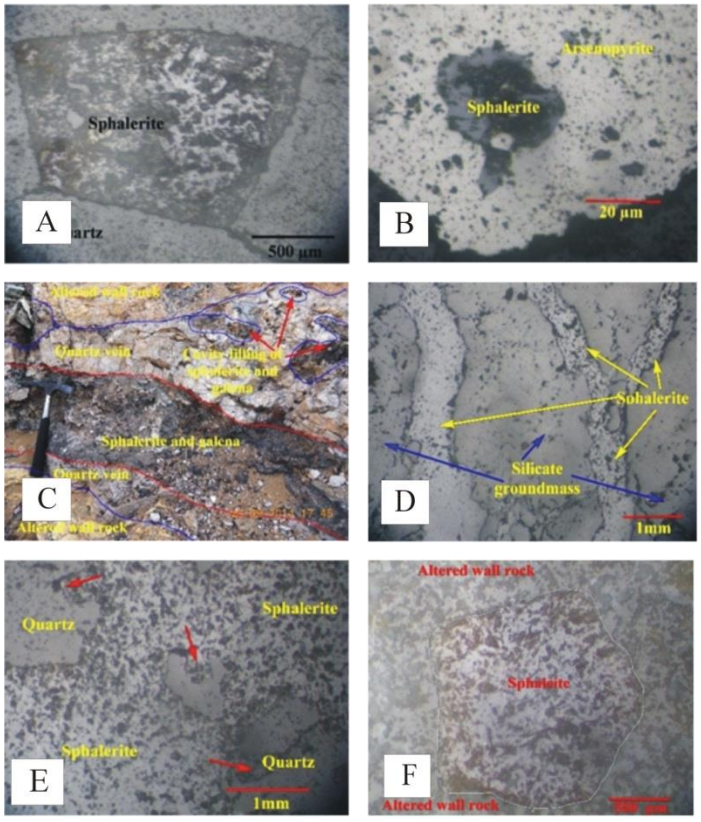

Figure 9. A) Euhedral to subhedral sphalerite-I occurs as disseminated crystals in quartz vein; B) Sphalerite-I occurs as inclusions within the coarse grained arsenopyrite; C) Sphalerite-II occurs in the form of fissure- and/or cavity-filling in the sheared quartz, in the central part of main quartz vein; D) Sphalerite-II occurs as fissure- -filling in the silicate groundmas; E) Sphalerite-II cements the quartz clasts and fragments, and their grain boundaries are corroded by sphalerite; F) Sphalerite-II shows occurs in the form of pseudomorphic euhedra, coarse-grained, in silicate groundmass.

pseudomorphic iron oxides formed due to oxidation of sulfide minerals (pyrite, arsenopyrite), (Figs. **11E** and **11F**), or associated with the oxidation of magnetite into iron oxides (Fig. **11G**) (3) Coarse-grained type of gold nuggets up to 70 µm is associated with sphalerite-II in fractured quartz vein and the wall rock alteration zones (Figs. **11H** and **11I**). EDS analysis of magnetite shows: Au (73.99 wt %) Ag (9.55 wt%), S (9.00 wt%), As (3.93 wt%), Fe (3.48 wt%) (Fig. **6G**).

5.3. Wall rock alteration

Two distinctive alteration zones can be regionalized around the mineralized quartz vein and shear zone, they are namely sericitic alteration and quartz- chlorite–epidote-pyrite.

5.3.1. Sericitic alteration zone

This alteration zone is characterized by the formation of secondary minerals such as sericite, muscovite, secondary quartz, and pyrite. These minerals assemblage replace the phenocrysts (plagioclase and K-feldspars) and ground mass. Intense alteration close to the mineralized quartz vein totally obliterated the rock textures. Sericite is the predominant alteration mineral in the alteration zone, where moderate to strong sericitization affected the feldspar phenocrysts and in

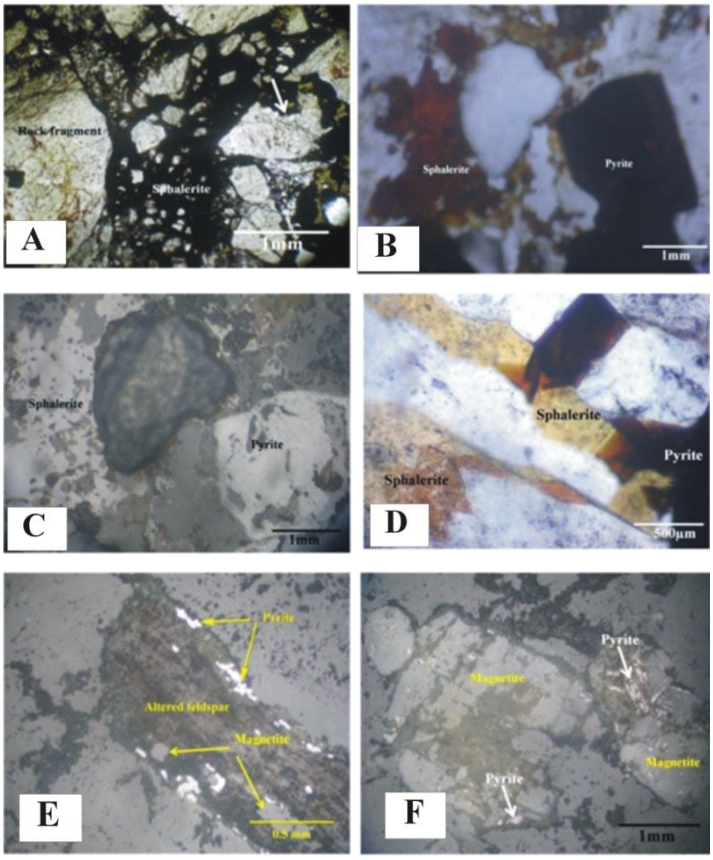

Figure 10. A) Sphalerite-II contains rock fragments of variable sizes and shapes of the country rocks, note the selectively replace the wall-rock clasts and along fractures and zones of weakness (white arrow); B) Sphalerite-II shows different shades of brown to reddish coloration when close to pyrite crystals, under transmitted light; C) the same veiw as B, under reflected light; D) Sphalerite-II shows variable coloration when close to pyrite crystals; E) magnetite inside plagioclase phenocrysts; F) magnetite aggregates of euhedral equant cubes, note replacement by pyrite.

the groundmass. Sericite makes up more than 40 percent of silicate alteration; the groundmass is more susceptible to alteration than the phenocrysts (Fig. 12A). Feldspar phenocrysts are altered to secondary sericite in variable scales, where the core of plagioclase is more susceptible to alteration than the grain boundaries.

Muscovitization is widespread in the dacitic country rocks, where coarse -grained, flaky muscovite replaces both K-feldspars and Plagioclase, with the K-feldspars being more transformed into muscovite (Fig. 12B). Muscovite replacing the phenocrysts usually shows no prevailed orientation along the cleavage of the feldspar crystals. Muscovitization also affected the sericitizied ground mass, in which, flaky secondary muscovite forms at the expense of the previously sericitized groundmass (Fig. 12C). In addition, secondary quartz forms nests a few millimeters in size and is composed of fine-grained anhedral interlocking grains (Fig. 12D). Phyllic alteration is characterized by the dissolution and replacement of earlier authigenic minerals, followed by partial filling of dissolution cavities. Abundant authigenic pyrite grains are wholly or partially surrounded by overgrowths of secondary quartz. This feature is known as pressure shadow and is commonly used to indicates pressure-solution phenomena. Pyrite (pyrite-II) is one of the most abundant alteration minerals in the alteration zone, occurring in a variety of size and forms; was described in the mineralogy section.

5.3.2. Quartz- chlorite–epidote-pyrite alteration zone

This alteration zone is represented by a narrow zone surrounding the sericite alteration zone, where the width of the zone does not exceed 1.5 meter.

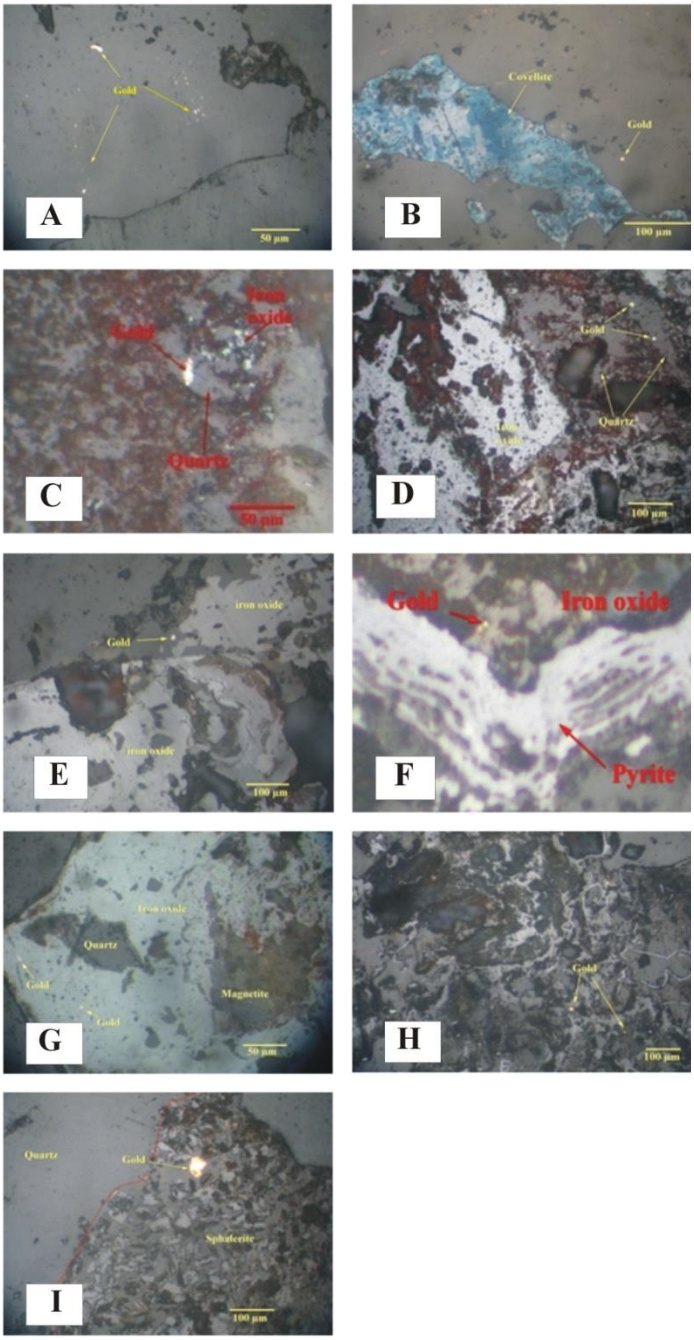

Figure 11. A and B) Gold disseminated in quartz vein; C and D) Gold assocaited with quartz clasts in breccia zone;E and F) Gold in the oxidation zones of the pseudomorphic iron oxides formed due to oxidation of sulfide minerals (pyrite, arsenopyrite); G) Gold associated with associated with the oxidation of magnetite in to iron oxides; H and I) Gold nuggets is associated with sphalerite-II.

It affects the ignimbrite and lava flow country rocks which underwent a strong chlorite–, epidote-, and pyrite-bearing alteration depicting the zone its characteristic greenish-yellowish tinge (Fig. 12E). The inner boundaries of the chlorite–epidote-pyrite alteration zone grades to sericite alteration zone while the outer boundaries grades to unaltered country rock. Chloritization is recognized in both the ignimbrite and the lava flows, where it occurs either as pseudomorphs after earlier ferromagnesian phenocrysts or as replacement in the groundmass (Fig. 12F). The calc-silicate alteration assemblage is dominated by epidote and to a lesser extent zoisite and saussurite. Epidote is formed at expense of the pre-existing plagioclase as a main saussuritization product. Epidote also represents an alteration product associated with chlorite formed at the expense of the pre-existing mafic minerals. Epidote is represented by many forms as equant euhedral individual grains or patches of fine-grained clusters (Fig. 12G). Epidote is observed in the alteration zone as elongate fracture-filling aggregates of epidote along shearing planes and cavities. Zoisite occurs as fine-grained mineral in association with the epidote (Figs. 12H and 12I).

Pyrite is an abundant mineral in this wall-rock alteration zone. It is observed as hypidiomorphic equigranular crystals formed at the expense of with chlorite and epidote. Sometimes it formed due to replacement of saussuritized plagioclase, and it occurs in the form of sub-idiomorphic crystals. Pyrite is commonly altered to hematite and goethite along the grain boundaries. Generally, the outer wall-rock alteration zones are stained by hematite, and is more or less impregnated with pyrite.

5.4. Geochemistry

Tables 1 and 2 show the major oxides, trace elements, and REE for the studied Dokhan Volcanics and granitic rocks, respectively.

5.4.1 Dokhan Volcanics

On the total alkali-silica (TAS) diagram [16], samples of the lower Dokhan Volcanic suite are plotted in andesite felid, while the Upper Dokhan Volcanic suite is restricted to rhyodacite and rhyolite fields (Fig. 13A).

The Hammad volcanics are dominantly medium-K, to high-K varieties (Fig. 13B). The studied lava flows represented by a sub-alkaline trend on total alkali-silica diagram (Fig. 13C) [16], and define the typical calc-alkaline trend on the AFM diagram (Fig. 13 D) [17]. Plots of the analyzed Dokhanvolcanic samples on (MgO–FeOt–Al_2O_3) diagram [18], showing that most of the samples, occupy the field of island arc and active continental margin basalts (Fig. 13E).The volcanic rocks plotted on Ti/100–Zr–Sr/2 diagram occupy and clothed to the field of "calcalkaline basalts (Fig. 13 F).

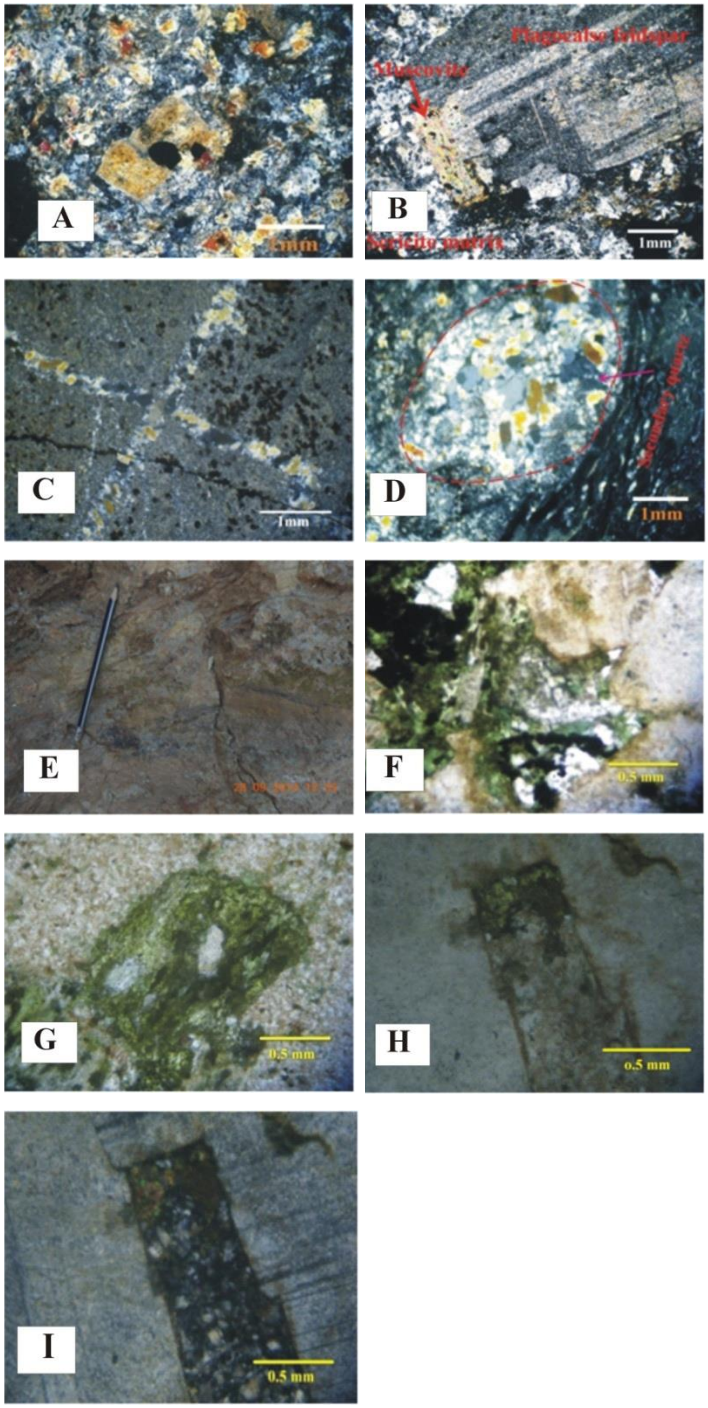

Figure 12. A) Sericite is the predominant alteration mineral in the alteration zone, note the groundmass is more susceptible to alteration than the phenocrysts;B) Musco-vitization, coarse -grained, flaky muscovite replaces plagioclase;C) silicification and secondary quartz in the form of a few millimeters quartz veins and stockworks; D) secondary quartz forms naests few millimeters in size; E) chlorite–, epidote-, and pyrite-bearingalteration depicting the zone its characteristic greenish-yellowish tinge; F) Chlorite occurs either as pseudomorphs after earlier ferromagnesian phenocrysts or as replacement in the groundmass; G) Equant euhedral individual epidote grain formed at the expense of the pre-existing mafic minerals; H) Zoisite occurs as fine-grained mineral in association with the epidote, under polarized light; I) the same view as H, under cross nicols.

5.4.2. Granite rocks

Using total alkalis versus silica (TAS) the classification diagram [16]and modified by [19] shows that all the samples occupy the field of granite (Fig. 14A) and all of the samples under investigation are of sub-alkaline affinity. According to $CaO–Na_2O–K_2O$ of [20] classification scheme, the studied samples spread over the granitic field (Fig. 14B). A total alkali-silica (TAS) diagram [21] and [17] showed that the samples plot in the granite fields (Fig. 14C).

Table 1. Major elements (in wt%) and trace elements (in ppm) composition of Dokhan Volcanics

	Rhyodacite									
	1	2	3	4	5	6	7	8	9	10
SiO_2	63.24	66.10	66.35	65.83	66.20	65.82	65.30	65.52	64.64	64.94
TiO_2	0.97	0.25	0.24	0.22	0.15	0.60	0.80	0.10	0.65	0.34
Al_2O_3	15.250	14.970	15.030	15.070	15.630	15.010	15.370	15.300	17.67	16.38
Fe_2O_3	6.39	3.60	2.92	3.04	2.65	2.05	2.65	2.63	3.08	3.24
CaO	4.2	3.1	4.1	3.4	2.1	3.0	3.3	3.4	4.32	4.27
MgO	3.00	2.31	2.19	2.17	2.01	2.71	1.95	2.17	1.91	2.14
Na_2O	4.44	4.89	4.41	4.37	4.83	4.36	4.47	4.40	4.52	4.1
K_2O	2.13	2.41	2.19	2.14	2.02	2.11	2.01	2.13	1.92	2.29
P_2O_5	1.04	1.20	1.20	1.20	1.10	1.00	1.12	1.00	0.5	1.12
L.O.I.	1.17	0.89	1.29	1.98	1.64	1.98	1.98	1.94	0.54	0.98
Total	99.8	99.69	99.90	99.41	98.31	98.65	98.97	98.61	99.75	99.8
Co	26	4	4	5	9	10	8	9	12	15
V	90	10	9	8	708	656	677	706	66	69
Cr	18	27	23	25	5	3	3	20	35	41
Ni	15	6	4	6	5	6	4	2	21	17
Cu	19	11	10	12	36	31	30	28	32	18
Zn	164	87	81	80	123	131	129	120	60	61
Pb	13	5	5	29	18	18	10	6	18	21
Ga	48	11	10	11	15	16	15	14	32	15
Rb	70	61	60	65	241	183	180	185	23	28
Sr	627	365	401	390	492	720	830	780	543	380
Ba	658	370	402	393	1028	1275	1211	1234	322	516
Zr	333	345	340	360	248	191	129	120	265	231
Y	15	16	14	15	12	17	15	14	15	17
Nb	20	8	7	6	2	1	2	6	5	6
U	1	3	5	2	3	2	3	5	6	6
Th	3	6	8	10	7	4	5	11	6	4

	Rhyodacite				Rhyolite				andesite			
	11	12	13	14	1	2	3	4	1	2	3	4	5
SiO_2	67.39	65.28	67.11	68.22	72.16	70.14	73.37	70.77	61.86	62.18	62.18	62.78	60.43
TiO_2	0.94	0.51	0.21	0.49	0.95	0.96	0.63	0.13	0.89	0.66	0.29	1.21	1.04
Al_2O_3	16.53	17.27	15.48	14.88	13.33	14.07	12.79	13.8	18.69	14.9	15.82	14.8	15.58
Fe_2O_3	1.56	3.88	2.97	2.05	1.67	1.88	0.73	2.05	3.8	5.59	4.39	5.38	6.16
CaO	2.64	2.74	3.54	3.14	0.83	0.25	0.31	0.16	4.01	6.4	5.6	4.2	4.14
MgO	2.33	2.11	2.22	2.17	0.35	0.92	0.15	1.57	2.22	3.09	3.65	3.10	3.27
Na_2O	4.13	4.11	4.02	4.82	4.15	3.88	4.65	4.52	4.73	3.78	3.44	3.35	3.67
K_2O	2.44	2.46	2.53	2.9	4.22	4.76	4.6	4.81	1.51	1.45	1.34	1.67	1.47
P_2O_5	0.89	1.01	1.3	0.7	0.7	0.9	0.02	0.30	0.42	1.39	1.39	0.72	1.21
L.O.I.	0.62	0.63	0.27	0.57	0.94	1.05	1.6	0.97	1.59	0.95	1.2	0.96	1.73
Total	99.47	100	99.65	99.94	99.3	98.81	98.85	99.03	98.72	99.94	99.69	99.17	98.7
Co	9	6	11	9	18	9	16	5	16	24	24	23	12
V	104	87	95	88	68	100	53	18	90	243	98	267	74
Cr	39	41	34	40	19	13	22	22	18	31	13	19	24
Ni	32	13	16	19	24	11	23	10	15	39	25	32	18
Cu	19	26	20	28	35	17	25	29	19	37	52	33	13
Zn	53	61	72	61	65	84	54	56	164	147	68	131	96
Pb	29	19	37	59	48	19	22	8	13	70	24	202	49
Ga	14	23	15	10	19	15	17	13	48	18	10	31	11
Rb	19	56	66	45	78	39	34	85	70	71	29	61	67
Sr	569	608	667	603	657	623	643	449	527	876	513	902	728
Ba	308	342	421	522	391	411	432	1367	656	447	243	1,139	667.8
Zr	279	187	185	225	190	89	224	3790	233	217	167	242	110
Y	18	15	20	17	19	19	14	17	15	14	16	18	18
Nb	5	7	11	9	9	5	5	16	8	3	4	3	8
U	2	5	1	3	4	1	5	4	5	3	7	1	3
Th	10	6	5	7	3	3	5	4	3	2	10	3	5

According to the SiO_2-CaO+Na_2O + K_2O diagram [22], the analyzed granitic rocks show mainly alkalic to alkalic-calcic characters (Fig. 14D). 100*(MgO+FeO*+TiO_2)/SiO_2 vs. (Al_2O_3+CaO)/(FeO*+Na_2O+K_2O) diagram [23] show that the present granitic rocks occupy the field of highly fractionated calc-alkaline(Fig. 14E). According to SiO_2 vs FeO/MgO diagram [24](Fig. 14F) the present granite rocks have I-type character, with only two samples plotted in the A-Type granite. In the Na_2O versus K_2O diagrams [25] the data from the study granite are consistent with I-Type granites (Fig. 15A).Using SiO_2 vs. A_2O_3 diagram [26] studied granite lies in the POG (post-orogenic granite) field (Fig. 15B).

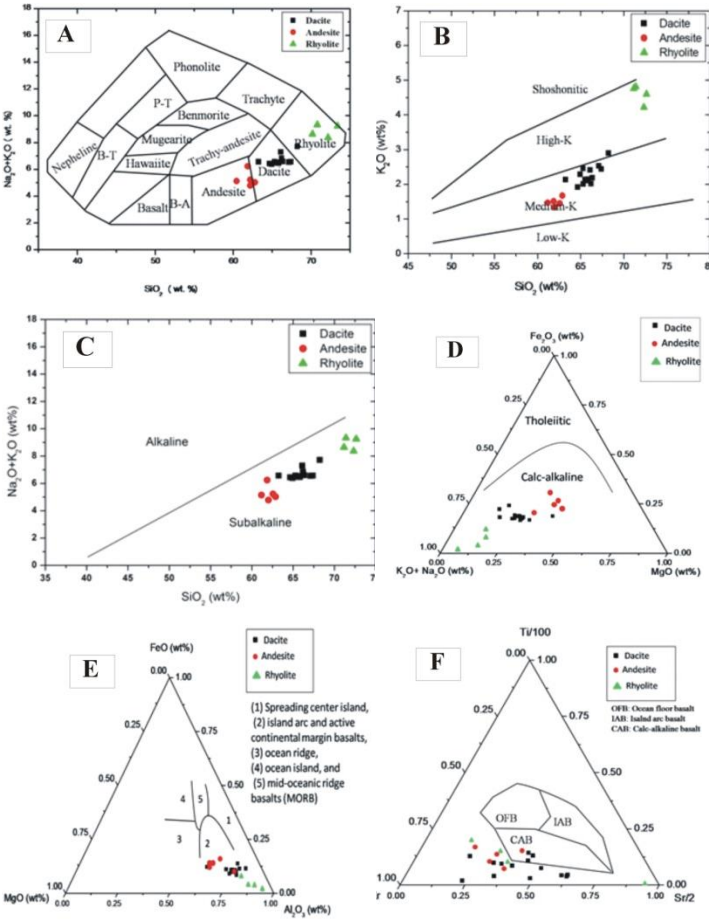

Figure 13. A) total alkali-silica (TAS) diagram for the analysed Dokhan volcanic rocks (Cox et al. 1979); B) Plots of the analysed Dokhan volcanics on the K2O vs. SiO2 (Preccerillo and Taylor, 1976); C) Plots of the analysed Dokhan volcanics samples on the Na2O+ K2O vs. SiO2 diagram (Irvine and Baragar, 1971; Cox et al. 1979); D) AFM diagram (Irvine and Baragar, 1971) for the analysed Dokhan volcanic rocks; E) Plots of the analyzed Dokhan volcanic samples on (MgO–FeOt–Al2O3) diagram of Pearce et al. (1977); F) plots the volcanic rocks samples on Ti/100–Zr–Sr/2 diagram (Pearce and Cann, 1973).

5.4.3. Mineralization zones

Geochemical analyses of the Hammad ore deposit generally show a very high Pb, Zn and Cu contents, averaging 2.01, 0.14 and 0.07 wt%, respectively, indicative of the abundant polymetallic mineralization [5, 7]; Au contents lies in the range of 0.19 up to 11.8 ppm with an average of 4.31 ppm, with presence of two very high readings of 156 and 199 ppm. Ag ranges from 6.8 up to 79.6 ppm with an average of 24.73 ppm, with presence of three readings of very high values of 300, 406.2 and 446.6 ppm (Table 3). For the content of the other trace elements: Sn, W, As and Mo are 12.26, 0.53, 0.72 and 3.16 ppm respectively. The average contents of Ni, Cr and V are 14.23, 2.52 and 14.48 ppm respectively (Table 3).

Table 2. Major elements (in wt %) and trace elements (in ppm) composition of granitic rocks

	1	2	3	4	5	6	7	8	9	10	11	12
SiO_2	71.22	72.89	75.58	71.65	73.28	73.83	72.45	75.61	76.67	77.55	74.34	74.56
TiO_2	0.41	0.31	0.16	0.34	0.39	0.33	0.32	0.12	0.19	0.122	0.24	0.29
Al_2O_3	14.90	13.29	13.12	14.16	13.48	12.65	13.55	12.56	11.96	12.19	12.95	12.89
Fe_2O_3	2.36	1.95	1.39	2.20	2.32	2.80	1.91	0.90	1.71	1.27	1.67	1.71
MnO	0.048	0.07	0.05	0.05	0.06	0.45	0.05	0.05	0.07	0.01	0.07	0.08
MgO	0.64	0.36	0.18	0.51	0.46	0.30	0.47	0.10	0.04	0.04	0.19	0.25
CaO	1.96	0.92	0.53	1.04	1.01	0.42	0.56	0.50	0.23	0.26	0.56	0.56
Na_2O	3.40	4.20	4.20	4.90	4.81	4.23	4.55	4.17	4.00	4.00	4.82	4.64
K_2O	4.39	4.24	4.46	3.94	3.67	4.07	4.36	4.52	4.50	4.41	4.51	4.48
P_2O_5	0.11	0.06	0.024	0.08	0.08	0.06	0.08	0.01	0.02	0.01	0.03	0.04
LOI	0.61	0.57	0.27	1.12	0.52	0.85	0.93	0.37	0.78	0.31	0.33	0.30
Total	99.75	98.82	99.98	99.84	100.04	99.35	99.21	98.93	100.10	100.10	99.75	99.79
Co	5.80	4.72	3.70	1.70	1.71	1.64	1.91	1.79	2.60	72.70	0.51	0.76
V	52.01	44.50	35.05	19.01	17.01	7.71	18.91	13.80	12.02	21.50	10.72	14.35
Cr	191.18	130.95	162.92	100.83	101.59	140.99	250.77	137.69	67.39	73.01	108.19	179.92
Ni	5.19	22.22	6.68	4.88	6.01	5.05	5.50	5.57	40.05	11.09	7.09	10.11
Cu	6.46	10.07	4.63	2.28	3.53	4.12	2.22	9.19	11.01	7.18	2.21	1.49
Zn	50.11	78.02	34.18	64.11	34.08	22.27	26.02	32.12	82.04	45.15	26.35	38.27
Pb	8.91	10.11	12.17	9.30	11.06	15.44	7.46	82.10	11.50	12.00	16.21	9.28
Ga	17.30	19.14	16.15	18.13	17.08	16.41	14.50	19.04	19.11	19.07	17.13	20.12
Rb	57.60	81.43	93.12	73.10	106.17	123.00	81.07	80.06	95.16	118.19	145.13	116.15
Sr	367.09	307.28	302.25	282.16	204.33	100.10	184.19	176.35	129.08	215.17	40.12	23.07
Ba	820.13	941.13	894.10	804.05	852.11	760.91	742.12	771.11	800.10	570.03	385.33	198.12
Zr	258.12	333.87	194.08	284.01	275.41	155.12	229.08	393.13	349.12	243.05	94.18	313.11
Y	24.18	25.07	14.18	30.10	21.14	16.28	15.15	33.15	36.10	22.10	15.90	32.00
Nb	12.11	12.80	12.50	12.50	12.14	13.41	11.60	15.10	15.45	15.60	12.37	17.06
U	1.61	2.59	3.77	2.16	3.96	4.43	3.36	2.62	3.50	4.14	4.22	3.28
Th	6.01	7.41	15.22	6.46	15.25	17.00	12.10	10.09	10.01	13.02	14.03	15.80

Table 3. Trace-element composition of the mineral-ization zone (in ppm)

No.	Au	Ag	Cu	Pb	Zn	Sn	W	Ni
1	6.6	300.0	667.8	14368	2137	13.1	0.21	35
2	2.6	79.6	3362	14675	1590	14.4	0.2	37
3	8.6	53.2	510	5633	166.6	11.7	0.3	33
4	2.1	6.8	82	1.4	9620	12.1	0.18	53
5	6.1	41	564.8	435	-	9.91	0.4	3.9
6	0.48	30.2	436.2	5694	349.8	10.1	0.3	4
7	199	406.2	1678	121360	3648	11.1	0.2	4.4
8	0.19	39.8	568.6	5844	192.6	12.00	0.5	4.5
9	0.24	16.2	288.8	6768	968	13.01	0.3	2.7
10	0.3	22.23	18.6	2992	692.4	13.3	0.31	3.1
11	11.9	16.2	320.4	5441	388	14.3	0.6	2.8
12	6.0	446.6	983	167640	2765	12.02	0.52	3.0
13	2.0	28.6	277.8	843.4	76.8	11.23	0.23	13.9
14	9	32.4	826.6	6134	1609	10.90	0.45	14.5
15	6.5	11.8	1132	1791	132	12.11	0.7	13.5
16	10	20.8	296.8	319	126.8	12.14	1.0	13.8
17	156.4	39.6	310	1734	240.2	14.02	2	6.9
18	5	6.8	191.4	671.2	706	13.2	1.1	7.1
No	As	Ti	Mo	Cr	V	Al	Mn	Ag/Au
1	0.9	52	4.4	1.5	4.9	6385	471	45.4
2	0.4	98	4	3.7	0.1	3505	260	30.6
3	0.4	61	3.6	4.0	2.4	1659	698	6.18
4	0.5	0.1	3.8	3.6	12.4	4744	977	3.23
5	0.9	75	2.7	2.1	27	1343	330	6.72
6	0.8	191	2.7	2.4	13	2245	277	62.9
7	0.7	121	2.6	3.0	20	2734	712	2.04
8	0.7	144	2.4	1.1	12.8	3921	640	
9	0.7	160	2.1	1.3	18	4037	298	67.5
10	0.6	0.1	3.2	2.4	12	4625	545	74.1
11	0.8	0.2	4.0	3.1	15	4811	528	1.36
12	0.9	0.4	4.1	2.3	14	3675	458	74.4
13	0.8	0.1	3.4	4.0	13	3471	371	14.3
14	0.7	0.1	2.4	3.1	19	2828	478	3.6
15	0.8	0.3	3.6	2.5	17	2414	616	1.81
16	0.8	0.5	2.5	1.5	24	1522	458	2.08
17	0.9	0.6	2.6	1.1	15	2551	534	0.25
18	0.6	0.4	2.8	2.7	21	2342	618	1.36

6. Discussion

Field geological studies show that the present mineralization is located in the contact between the Dokhan volcanic and the younger granite along the shear zone between them. Dokhan volcanic rocks are represented by andesite and rhyodacite and rhyolite varieties; they exhibit calc-alkaline magma type related to

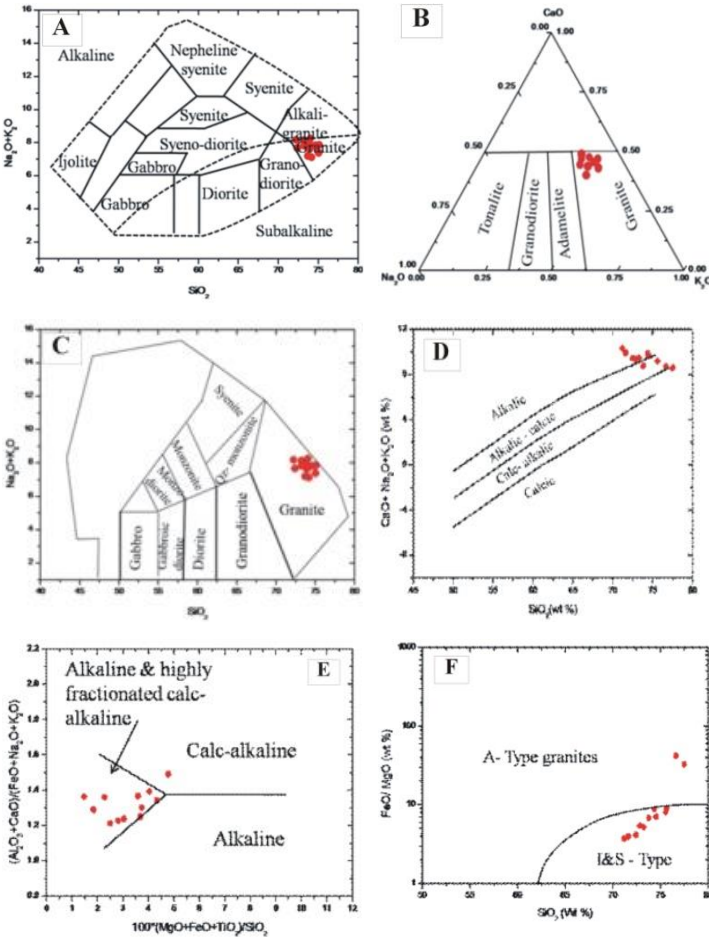

Figure 14. A) total alkali-silica (TAS) diagram for the analysed granite rocks (Cox et al. 1979); B) CaO–Na_2O–K_2O classification scheme of Archibald et al. (1981), for the studied granitic rocks; C) A total alkali-silica (TAS) diagram after Le Bas et al. (1986) and Irvine &Baragar (1971) plots of the granite rocks; D) SiO_2-CaO+Na_2O + K_2O diagram of Frost et al. (2001), of the analysed granitic rocks; E diagram of 100*(MgO+FeO*+TiO_2)/SiO_2 vs (Al_2O_3+CaO)/(FeO*+Na_2O+K_2O) (after Sylvester, 1989) of the present granitic rocks; F) SiO_2 vs. FeO/MgO diagram (Eby 1990) of the present granite.

island arc system.However, granitic rocks are of I-type granites composition with highly fractionated calc-alkaline affinity developed in post-orogenic granite regimes. Four main types of mineralization styles are recognized they are; 1- mineralized quartz vein, 2- hydrothermal wall rock alteration, and 3- breccia. The geological studies indicate that the present mineralization belongs to the intrusion-related gold deposits [4]. Generally, the hydrothermal deposits have relatively low Ni/Cr ratios owing to the higher solubility of Ni with respect to Cr in hydrothermal fluids [27]. Therefore, the diagrams of Ti versus Ni/Cr and Cr versus V [28] are used to distinguish between hydrothermal and igneous origin of sulfide deposits[29]. Plotting of the present samples on the Ti versus Ni/Cr and Cr versus V reveals that all samples are plotted in the hydrothermal fields (Figs. 16A and 16B). Distinctive features such as volcano-plutonic host rocks of calc-alkaline affinity at convergent margins, existence chalcedonic quartz, calcite, and hydrothermal breccias, a characteristic elemental association such as Au, Ag, As, Pb, Zn and Cu, in addition to

characteristic ore textures such as open-space filling, crustification, colloform banding and comb structures, all are indicative for epithermal mineralization [30]. Moreover, regarding the high gold contents in the studied deposit, plotting of the samples on the ternary diagram of [31] which shows the compositional ranges for common geologically-defined types of hydrothermal ore deposits, the present samples lie in the field of most epithermal gold deposits (Fig. 16C). In contrast to most gold-bearing quartz veins in the Eastern Desert of Egypt, the Hammad gold-bearing quartz vein however contains few amounts of Pb, Zn and Cu (Table 3). Plotting samples of the present deposit on the diagram [32, 33], the samples of Hammad deposit lie in the Pb-Cu field (Fig. 16D). Open-space veins, breccias and stockworks, gangues of quartz, chalcedony, and calcite in addition to colloform banding, hydraulic fracturing, the relatively low concentrations of Cu and other base metals, and the presence of the mineralization inside the volcanic suite or at its contact with granite, all indicate the low sulphidation nature of this epithermal deposit[30]. The authors [29] used the (Ti+V) vs (Al+Mn) diagram where the temperature is a controlling factor for trace element incorporation in the hydrothermal minerals. Plotting of Hammad deposit samples on this diagram reveals that the present deposit was formed under a temperature range of 200-300 °C (Fig. 16 E). The author [34] used the Ag/Au ratio as an important factor for determining the metallogenic nature of the epithermal system. Accordingly, epithermal systems with sulfide complexing would be dominated by native gold and electrum and show homogenization temperatures less than 250 °C when Ag/Au ratios ≤1. If the ratio of Ag/Au is > 1, the hydrothermal system would be characterized by chloride complexing, dominated by base-metal sulfides and sulfosalts and electrum, with minor Au and temperatures of homogenization are greater than 250 °C [30]. For Hammad deposit the Ag/Au ratio is> 1, and thus the deposit was deposited from a hydrothermal system with chloride complexing, with a homogenization temperature greater than 250 °C and dominated by base-metal sulfides and sulfosalts and electrum, with minor Au. When the Ag/Au ration is 1-10, then the deposit is Au-rich, while high Ag/Au ratio ~100, then the deposit is Ag-rich. Accordingly, the Hammad deposit can be classified as Ag-rich low-sulphidation deposit where its Ag/Au ratio averaging 22 up to 74.1 (Table3).

Model of mineralization

On the basis of the paragenetic sequences, ore fabrics, and crosscutting relationships, the present ore deposit was formed in three stages.

The first stage is associated with the initial shearing along the contact between the granitic rocks and Dokhan Volcanic. During this stage, the main milky white quartz–polymetallic sulfide vein was formed including (arsenopyrite, pyrite-I, chacopyrite-I, sphalerite-I, galena-I). This main quartz vein was formed due to extensive silicification of the wallrock along the shear zone [5]. Development of the quartz vein took place in multistage impulses. The N-S trending sinistral shear zone represented the pathway for the mineralizing hydrothermal solutions related to the post tectonic younger granite. The country rocks around the main quartz vein suffered from sericite alteration, where the country rocks was locally intensely replaced by sericite and fine-grained muscovite, secondary quartz and pyrite crystals are also can be observed. The quartz-forming solution was of reducing nature as indicated by the formation sulfide assemblage in quartz vein and formation of pyrite in alteration zone at the expense of magnetite plagioclase and muscovite. Backscattered electron images revealed the presence of minute gold nuggets associated with the fine grained galena, sphalerite and chalcopyrite inside the arsenopyrite crystals (Fig. 17A). This gold is thus has been transported as $Au(HS)_2$ bisulfide complex [35].

The second stage is associated with the third and fourth deformational events affected the mine area. The third extensional dextral faulting and shearing in the ENE-WSW direction caused displacement of the mineralized zone and the contact between the younger granites and Dokhan Volcanics. This extension is responsible for the formation of the bimodal dike swarms in the Eastern Desert [36], and represented in the mine area by basic dolerite dykes which crosscut the early formed quartz vein. The fourth compressional deformational event caused the formation of two conjugate sets of shear fractures sets, a predominant trending WNW-ESE dextral faults and shearing and another NNW-SSE sinistral faults and shearing. These shearing inside the quartz veins, along with the invasion of hydrothermal solutions related to the dolerite (basic) dykes led to formation of the grey colored, fine grained brecciated and/or laminated saccharoidal Au-rich quartz, intervened and cemented by sphalerite-II. This stage is also characterized by the alteration of arsenopyrite and pyrite-I into pseudomorphic iron oxides, alteration of chalcopyrite into covellite. Alteration of arsenopyrite and pyrite-I into pseudomorphic iron oxides is contemporaneous with the release of gold and its precipitation in quartz vein along and close to fissures and minute fractures or associated with quartz fragments [37-39];(Fig. 17B). Base metals are favorably transported in the hydrothermal solutions as chloride complexes [40]. The pervasive formation of the cavity and/or fracture-filling sphalerite-II indicate that the hydrothermal solution was Zn-rich most probably transported as chloride complexes. Coarse-grained gold that is confined only to sphalerite-II [41], is consequently most probably transported as chloride complex. During this stage, distal parts of the country rocks around the quartz vein were affected by chlorite-epidote-pyrite alteration.

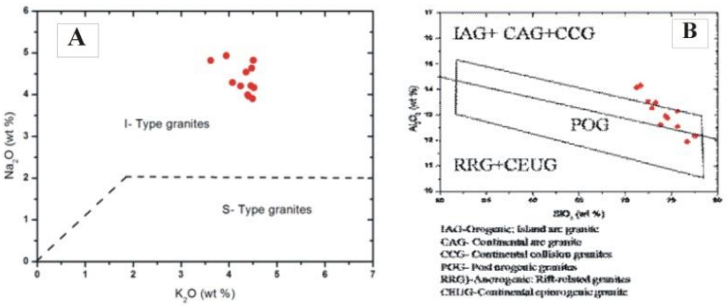

Figure 15. A) Na_2O versus K_2O diagrams (Chappell and White, 1974) of the granite; B) SiO_2 vs. A_2O_3 diagram after Maniar and Piccoli (1989) of the studied granite.

The third stage is represented by weathering of the ore minerals under surface conditions leading to the formation of cerussite, smithsonite malachite, and goethite. In hydrothermal conditions, gold is favorably transported as bisulfide complex $Au(Hs)_2$[35]. While base metals are favorably transported as chloride complexes[40]. [42] interpreted the association of gold with galena in pyrite by mixing of base metal-bearing chloride complex with precious metal-bearing bisulfide ones that would destabilize them triggering both gold and base metal deposition.

7. Conclusion

(1) Wadi Hammad mineralization is hosted in the contact between Dokhan volcanics and Younger granite. Dokhan volcanicsare erupted ascalc-alkaline magma type in island arc system. However, Younger granitic rocks are of I-type granites with highly fractionated calc-alkaline affinity developed in post-orogenic granite regimes.

(2) The mineralization follows the main shear zone trending N-S direction and represented by a mineralized quartz vein, alteration zones, and breccias. The mineral assemblage is arsenopyrite, pyrite, galena, sphalerite, and gold, this assemblage referred to as epithermal type, the alteration products of the main sulfide minerals are Pb, Zn, and Cu carbonate and oxides (iron oxides, cerussite, smethsonite, covellite, bornite and malachite). The alteration zones bounded the main mineralized vein are cerussite and chlorite-epidote-pyrite zones.

(3) Geochemical studies indicate that this mineralization is formed due to hydrothermal solutions may be related to intrusion of younger granite and dolerite dykes, the mineralization is of Ag-rich, low sulphidation epithermal gold deposit type, formed at a temperature range of 200-300 °C.

(4) Hammad mineralization is structurally controlled, and it is suggested that it was formed in three stages;

(5) The first stage; is due to the intrusion of younger granite into the Dokhan Volcanics coeval with the initial shearing along the contact between them and resulting in the formation of a N-S trending shear zone. Hydrothermal solutions related to the younger granite intrusion follow the shear zone producing the main milky white quartz–polymetallic sulfide vein including (arsenopyrite, pyrite-I, chalcopyrite-I, sphalerite-I, galena-I).

(6) The second stage is associated with the third and fourth deformational events affected the mine area. The third extensional dextral faulting and shearing in the ENE-WSW direction is responsible for the formation of basic dolerite dykes which crosscut the early-formed quartz vein. The fourthcompressional deformational event caused shearing and fractures of the early formed quartz veins, along with the invasion of hydrothermal solutions related to the dolerite (basic) dykes led to the formation of the grey colored, fine grained brecciated and/or laminated saccharoidal Au-rich quartz, intervened and cemented by sphalerite-II. This stage is also characterized alteration of arsenopyrite and pyrite-I into pseudomorphic iron oxides is contemporaneous with the release of gold and its precipitation in quartz vein along and close to fissures and minute fractures or associated with quartz fragments.

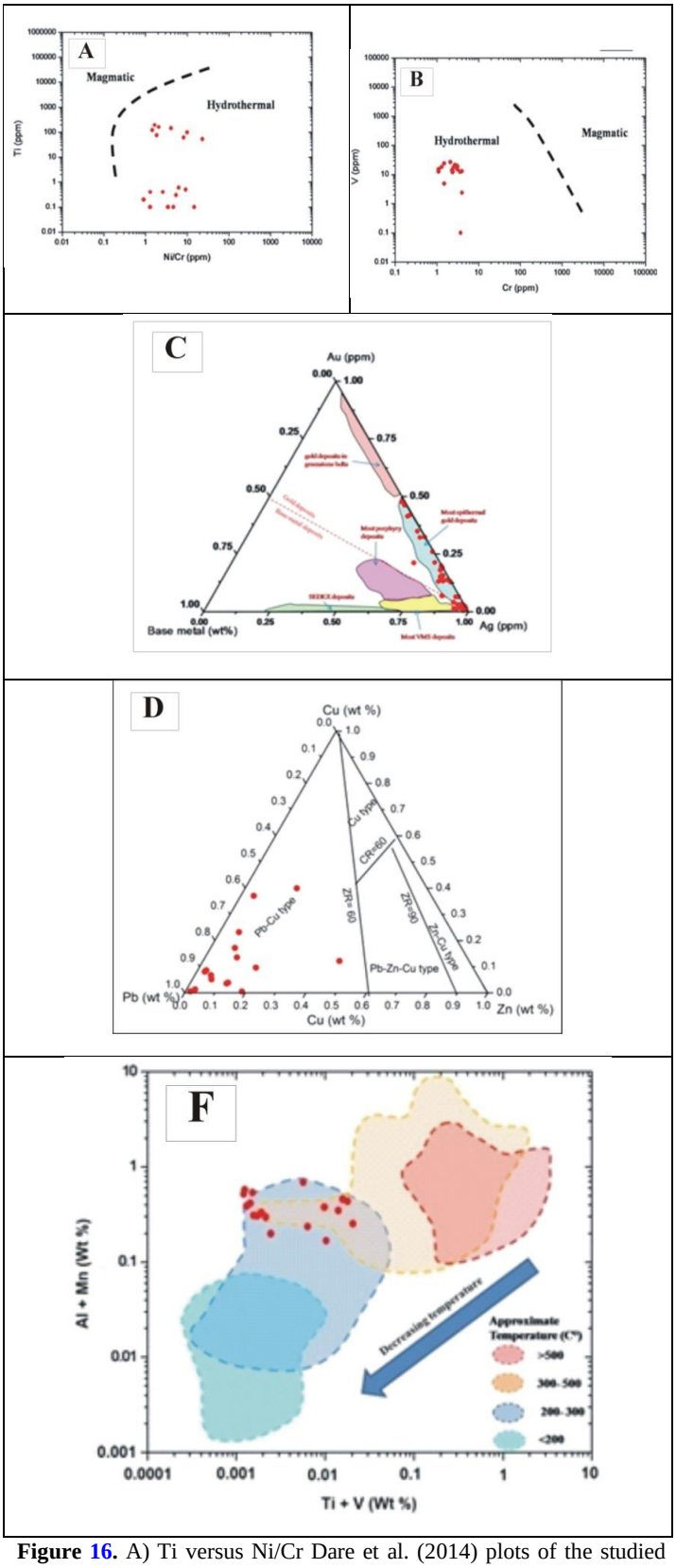

Figure 16. A) Ti versus Ni/Cr Dare et al. (2014) plots of the studied mineralization; B) Cr versus V of Dare et al. (2014) plots samples of Hammad mineralization; C) Plots of the studied deposit samples on the ternary diagram of (Poulsen, 1995); D)); Plotting Hammad deposit samples on the diagram of (Franklin et al., 1981 and Franklin, 1993); E) Plotting Hammad deposit samples on the (Ti+V) vs (Al+Mn) diagram of Han et al., (2022).

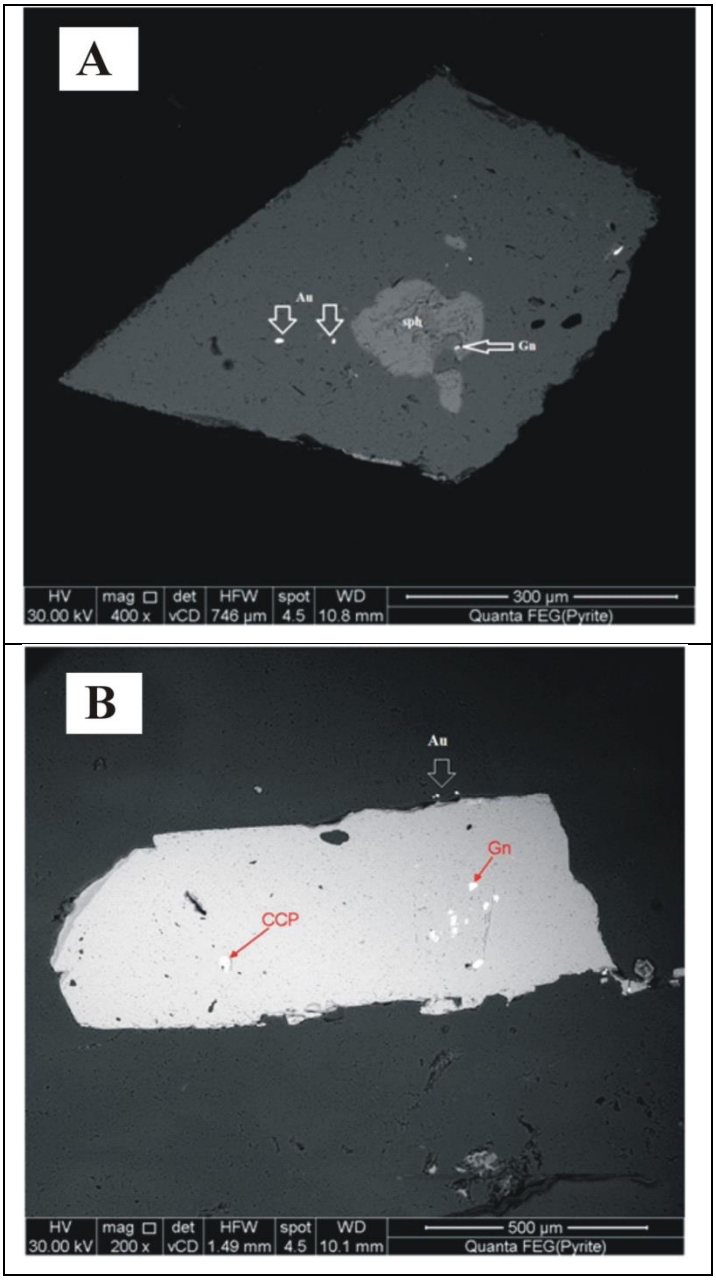

Figure 17. A) Back scattered electron image in aresenopyrite showing presence of minute gold nuggets (Au) associated to the fine grained galena(Gn), and sphalerite(sph)inside the aresenopyrite crystal; B) Back scattered electron image in aresenopyrite showing presence of minute gold nuggets (Au) in quartz closely beside the arsenopyrite. Note presence of fine grained galena (Gn), and chalcopyrite (CCP) inside the aresenopyrite crystal.

(7) The third stage is due to oxidation and weathering of the sulfide minerals forming secondary minerals including cerussite, smethonite covellite bornite and malachite.

(8) Results of this study reveals that the North Eastern Desert (NED) of Egypt contains promising gold deposits in contrary to the speculation that the NED was for long time devoid from gold mineralization, and thus the present study is setting the stage for future exploration for gold in the NED.

(9) The present study unveiled the nature of intrusion-related type of mineralization and their characteristic features which can be used in exploration of similar types in the surrounding areas.

References

[1] R. Sillitoe, in Gold metallogeny and exploration. 1991, Springer. p. 165-209.

[2] N.S. Botros, in: The Geology of the Egyptian Nubian Shield., Springer. 2021, p. 549-575.

[3] B.A. Zoheir, *Microchemical Journal*, 2012. 103: p. 148-157.

[4] N.S. Botros, *Acta Geologica Sinica-English Edition*, 2021. 95(3): p. 1033-1055.

[5] K. I Khalil, M. El-Roz, M.H. Shalaby and A.I. Arslan,. *International. Conference on geochemistry, Alex. Univ., Egypt*, V. I, 169-190. , 2006.

[6] Osman, A., In: A. Stanly et al. (eds.) Mineral deposits: possessing. Balkema, Rotterdam, 189-192. . 1999.

[7] B.B. Nasr, M.S. Masoud, H. El Sherbeni and A.A. Makhlouf, *Annals of Geological Survey of Egypt*, 1998. 21: p. 331-344.

[8] A. Osman, H. Kucha, and A. Piestrzynski, *Mineralogia Polonica*, 2000. 31(2): p. 17-30.

[9] F.H. Mohamed, and M.M. El-Sayed, *Geochemistry*, 2008. 68(4): p. 431-450.

[10] A.M. Abdel-Rahman, *Geological Magazine*, 1996. 133(1): p. 17-31.

[11] H. Khamis, M. Sc. Thesis, Cairo Univ. 235p. 1995.

[12] F.F. Basta, A.E. Maurice, B.R. Bakhit, M.K. Azer and A.F. El-Sobky, *Lithos*, 2017. 288: p. 248-263.

[13] E.A. Khalaf, *Bulletin of volcanology*, 2013. 75(2): p. 1-31.

[14] R.J. Stern, *Annual review of earth and planetary sciences*, 1994. 22: p. 319-351.

[15] H.I. El Sundoly, I. H. Azab, and H. Khamis, *Annals of Geological Surveyof Egypt*. V. XXXVIII, pp. 97 - 111., 2021.

[16] K.J. Cox, J.D. Bell, and R.J Pankhurst, in: The Interpretation of Igneous Rocks, Springer. 1979, p. 12-41. 1979

[17] T.N. Irvine, and W. Baragar, Canadian journal of earth sciences, 1971. 8(5): p. 523-548.

[18] T.H.Pearce, B.E. Gorman, and T.C. Birkett,. Earth and Planetary Science Letters, 1977. 36(1): p. 121-132.

[19] M. Wilson, Igneous Petrogenesis: a global tectonic approach . The Netherlands, Springer. 2007

[20] N. J,Archibald, L.F. Bettenay, M.J. Bickle, D.I. Groves, . Archean geology, 1981. 7: p. 491-504.

[21] M.J. Le BAS, R.W. Le Maitre, andA. Streckeisen and B.

Zanettin, *Journal of petrology*, 1986. 27(3): p. 745-750.

[22] B.R. Frost, C. G. Barnes, W.J. Collinis, R.J. Arculus, *Journal of petrology*, 2001. 42(11): p. 2033-2048.

[23] P.J. Sylvester, *The Journal of Geology*, 1989. 97(3): p. 261-280.

[24] G.N. Eby, *Lithos*, 1990. 26(1-2): p. 115-134.

[25] B. Chappell, and A. White, *Pacific Geology*, 8, 173-174. 1974.

[26] P. Maniar, and P. Piccoli, *Geological Society of America Bulletin*, 101 (1989), 635-643. 1989.

[27] E. Boutroy, S.A.S Dare, G. Beaudoin, S-J. Barnes, P.C. Lightfoot, *Journal of Geochemical Exploration*, 2014. 145: p. 64-81.

[28] S.A.S. Dare, S.J. Barnes, G. Beaudoin, J. Méric, E. Boutroy, C. Potvin-Doucet, *Mineralium Deposita* 49 , 785-796, 2014.

[29] C-C. Han, X-B. Zhang, S-S. Wu, and Y-T. Liu, *Minerals*, 2022. 12(4): p. 485..

[30] F. Pirajno, Hydrothermal Mineral Deposits, Principles and Fundamental Concepts for the Exploration Geologist. 1992 Edition, 2009 Springer, p. 706.

[31] K. Poulsen, Lode gold. In:O.R. Eckstrand, W.D Sinclair,. and R.I. Thorpe, (eds.) Geology of Canadian mineral deposit types (P-1), no. 8, p. 323-328. 1995.

[32] J.M. Franklin, 1993, in:RV. Kirkham, W. D. Sinclair, R.I. Thorpe, and J.M. Duke, J.M., eds., Mineral deposit modeling, Geological Association of Canada Special Paper 40, p. 315- 34. 1993

[33] J.M. Franklin, D.M. Sangster, and J.W. Lydon, *Economic Geology, 75th Anniversary Volume, 1981, Economic Geology Publishing company, Lanscate, Pa.*

[34] D. Cole, and S. Drummond, *Journal of Geochemical Exploration*, 1986. 25(1-2): p. 45-79.

[35] T. Seward, in Gold Metallogeny and Exploration (R.P. Foster, editor). Blackie, Glasgow,UK. pp 39-62. 1991

[36] R. G. Stern, G. Sellers, and D. Gottfried. In: S. El Gaby, and R. O. Greiling, Eds., The Pan-African Belt of Northeast Africa and Adjacent Areas, Vieweg, Weisbaden, 147-177. 1988.

[37] Osman, A., *Middle East Research Center, Ain Shams University, Earth Science Series.* 1994. p. 74-87.

[38] A. Mumin, M. Fleet, and S. Chryssoulis, *Mineralium Deposita*, 1994. 29(6): p. 445-460.

[39] M.E. Hilmy, and A. Osman,*Mineralium Deposita*, 1989. 24(4): p. 244-249.

[40] H.L. Barnes, Geochemistry of hydrothermal ore deposits. 1997: John Wiley & Sons.

[41] B. Zoheir, B.F. Deshesh, C. Broman and I Pitcairn, *Mineralium Deposita*, 2018. 53(5): p. 701-720.

[42] O. Kreuzer, *Mineral. Deposita*, 40, 639-663. 2006.